

1 Supplementary Information

2 **Title:** Engineering TadA ortholog-derived cytosine base editor without motif
3 preference and adenosine activity limitation
4

5 **Authors list:**

6 Guoling Li^{1†}, Xue Dong^{1†}, Jiamin Luo^{1†}, Tanglong Yuan^{2†}, Tong Li^{1†}, Guoli Zhao^{3,4†},
7 Hainan Zhang¹, Jingxing Zhou¹, Zhenhai Zeng^{3,4}, Shuna Cui¹, Haoqiang Wang¹, Yin
8 Wang¹, Yuyang Yu¹, Yuan Yuan¹, Erwei Zuo^{2*}, Chunlong Xu^{5*}, Jinhai Huang^{3,4*}, Yingsi
9 Zhou^{1*}

10
11 **Affiliations:**

12 ¹HuidaGene Therapeutics Co., Ltd., Shanghai 200131, China

13 ²Shenzhen Branch, Guangdong Laboratory for Lingnan Modern Agriculture, Key
14 Laboratory of Synthetic Biology, Ministry of Agriculture and Rural Affairs, Agricultural
15 Genomics Institute at Shenzhen, Chinese Academy of Agricultural Sciences, Shenzhen,
16 China.

17 ³Eye Institute and Department of Ophthalmology, Eye and ENT Hospital, Fudan University,
18 Key Laboratory of Myopia, Chinese Academy of Medical Sciences, Shanghai, 200030
19 China

20 ⁴Shanghai Research Center of Ophthalmology and Optometry, Shanghai, 200030 China

21 ⁵Lingang Laboratory, Shanghai, China.

22 [†]These authors contributed equally to this work.

23 ^{*}Corresponding authors. zuoerwei@caas.cn (E.Z.); xucl@lglab.ac.cn (C.X.);
24 jinhaihuang@fudan.edu.cn (J.H.); yingsizhou@huidagene.com (Y.Z.)

25

26

27

28

29

30

31

32

33

34 **This PDF file includes:**

35 **Supplementary Figure 1 to 11**

36 Supplementary Fig.1 Sanger sequencing of AjTadA.v1 at PIK3CA loci.

37 Supplementary Fig.2 Conservative site analysis of TadA protein sequence
38 based on multiple sequence alignment.

39 Supplementary Fig.3 ATdCBE enables robust C-to-T genomic editing in
40 mammalian cells.

41 Supplementary Fig.4 A-to-G genomic editing of base editors in mammalian
42 cells.

43 Supplementary Fig.5 AjTadA-derived base editors with high specificity in
44 mammalian cells.

45 Supplementary Fig.6 Compare the editing products of the base editors without
46 UGI at three endogenous loci.

47 Supplementary Fig.7 Comparing the editing efficiency of CBEs at the exon 55
48 SAS of DMD gene in HEK293T cells.

49 Supplementary Fig.8 Establishment and characterization of a humanized DMD
50 mouse model.

51 Supplementary Fig.9 Rescue of dystrophin expression following intramuscular
52 injection of aTdCBE after 6 weeks.

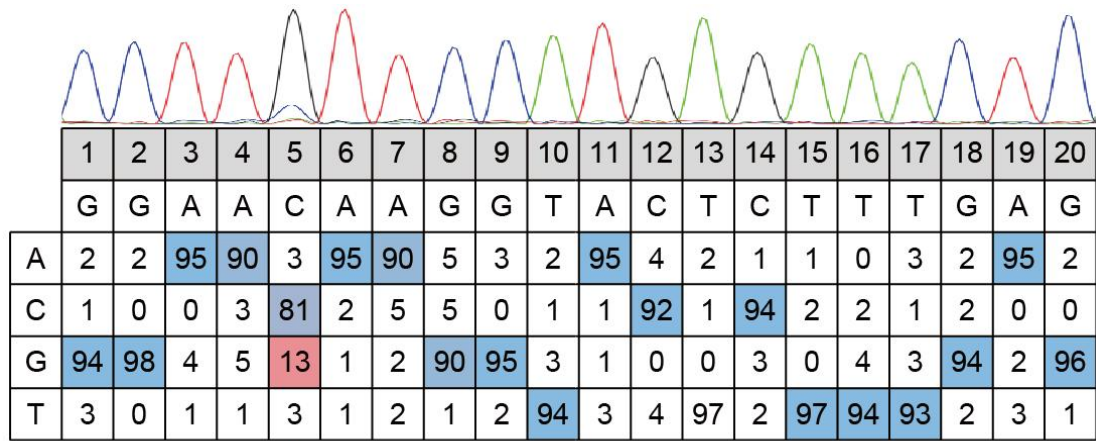
53 Supplementary Fig.10 Uncropped images.

54 Supplementary Fig.11 Flow cytometry gating strategy.

55

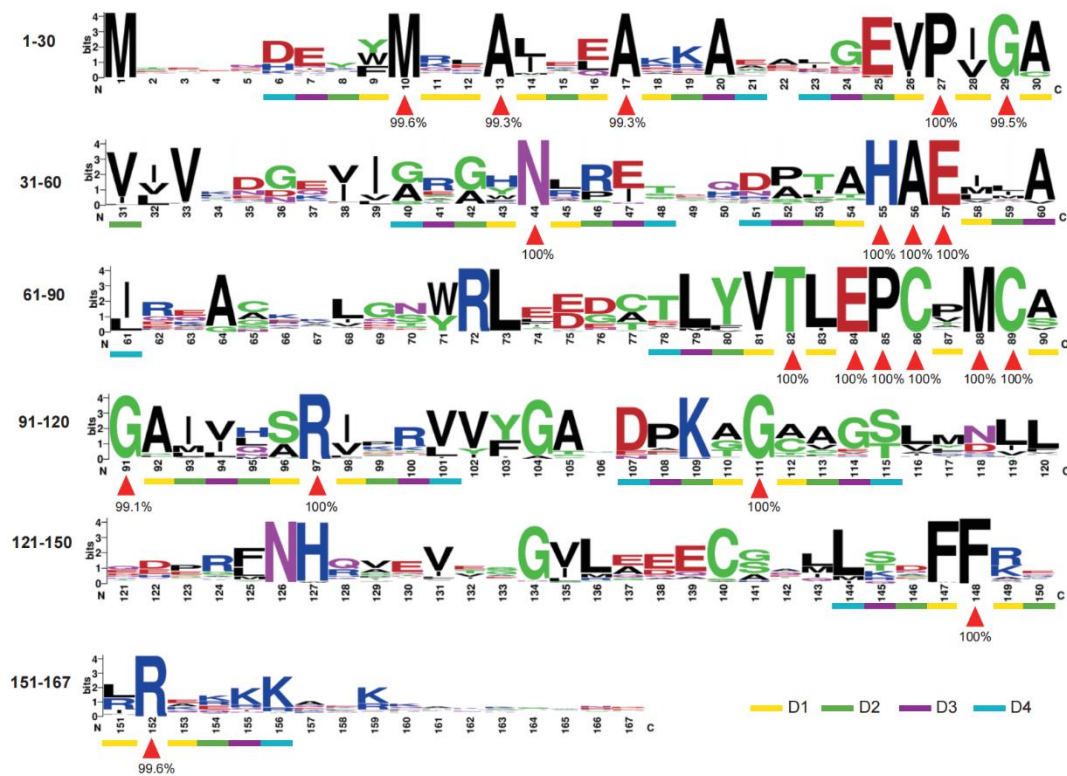
56

57



58
59
60

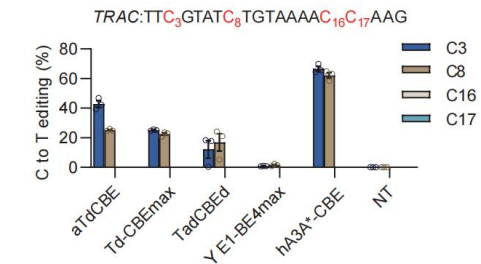
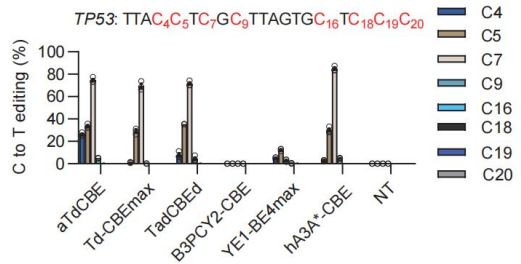
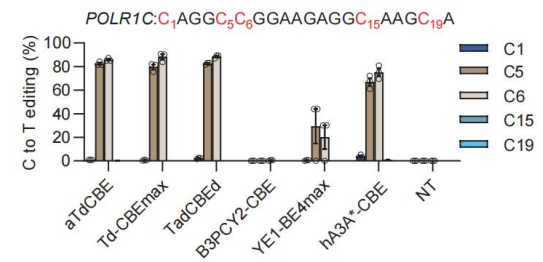
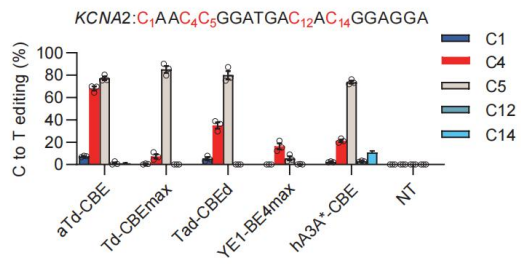
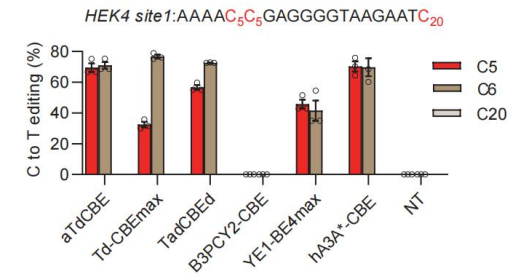
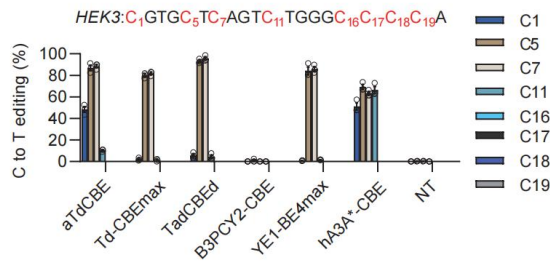
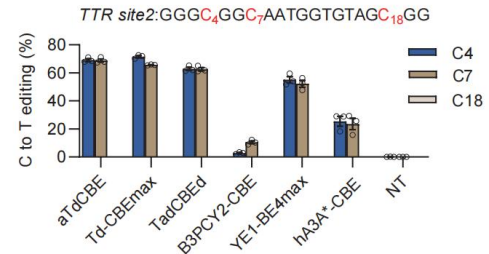
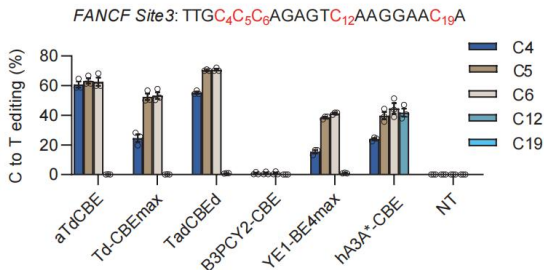
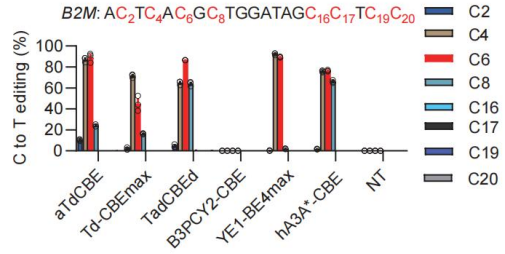
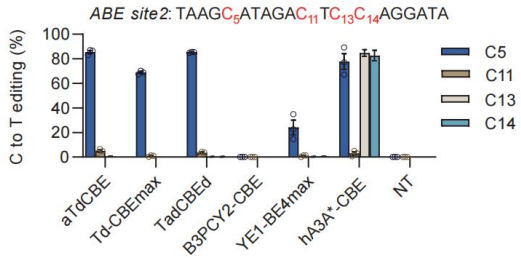
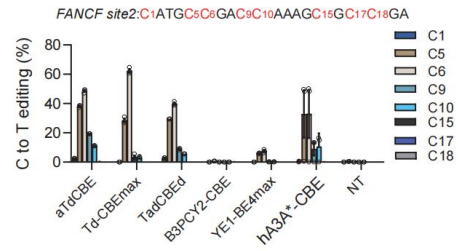
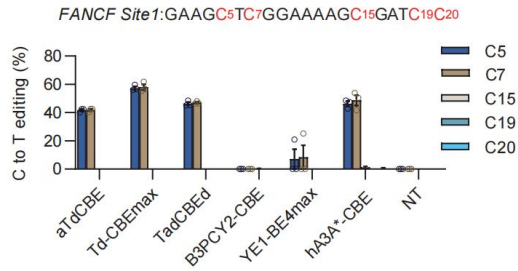
▲
Supplementary Fig.1 Sanger sequencing of AjTadA.v1 at *PIK3CA* loci.

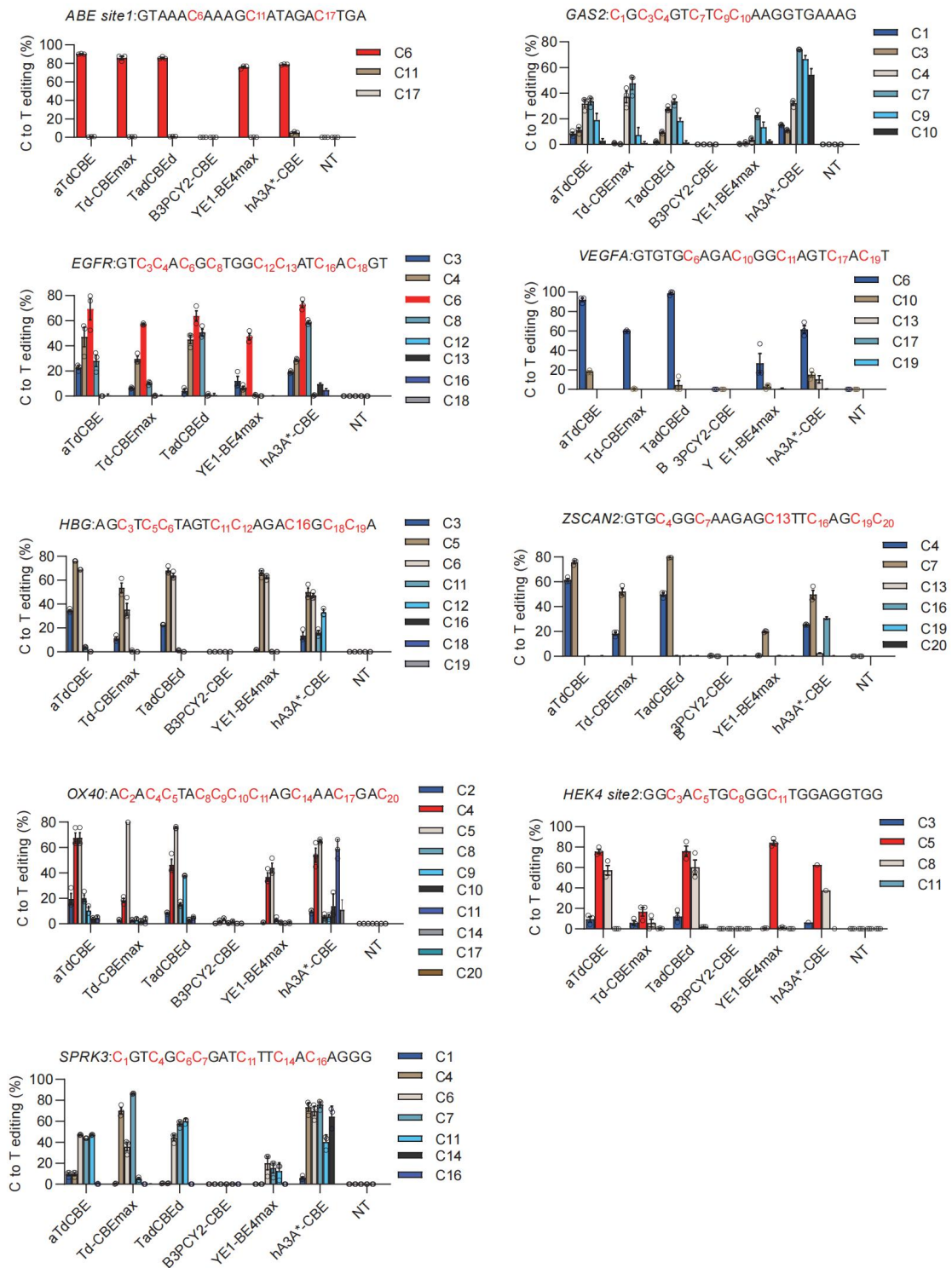


61
62
63
64
65
66
67
68

Supplementary Fig.2 Conservative site analysis of TadA protein sequence based on multiple sequence alignment.

The red triangle indicates highly conserved amino acids. The yellow, green, purple and blue squares represent adjacent amino acids with different distances from highly conserved sites. The amino acid frequency visualized by weblogo(<https://weblogo.berkeley.edu/logo.cgi>).

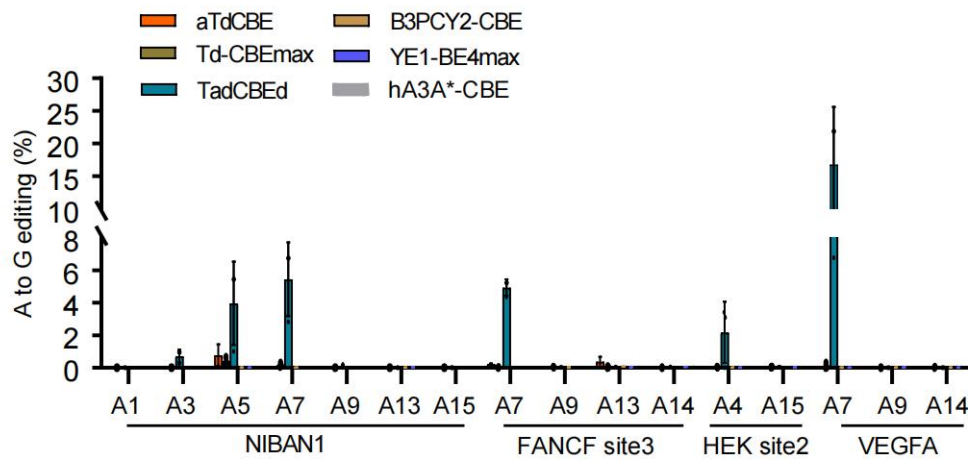
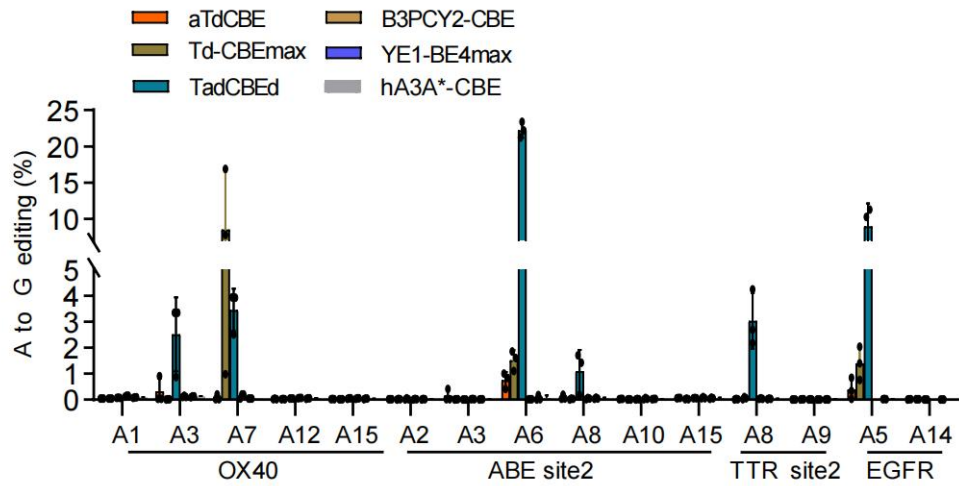




71

72 **Supplementary Fig.3 ATdCBE enables robust C-to-T genomic editing in**
 73 **mammalian cells.**

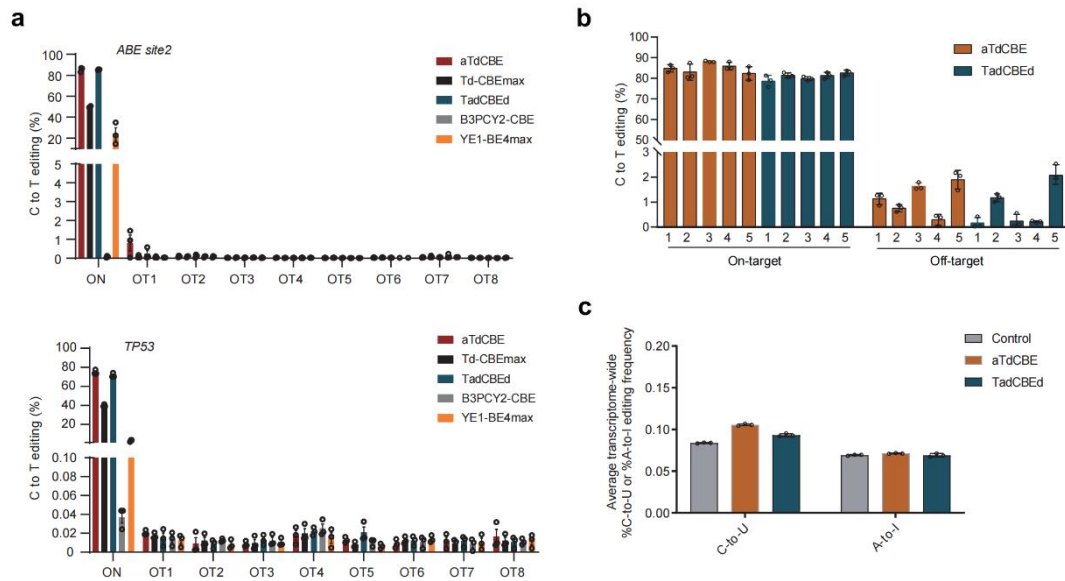
74 Data are presented as means \pm S.D. Values represent n = 3 independent
 75 biological replicates. All of the above base editors contain UGI.
 76 Source data are provided as a Source Data file.



77

78 **Supplementary Fig.4 A-to-G genomic editing of base editors in**
 79 **mammalian cells.**

80 Data are presented as means \pm S.D. Values represent n = 3 independent
 81 biological replicates. All of the above base editors contain UGI.
 82 Source data are provided as a Source Data file.

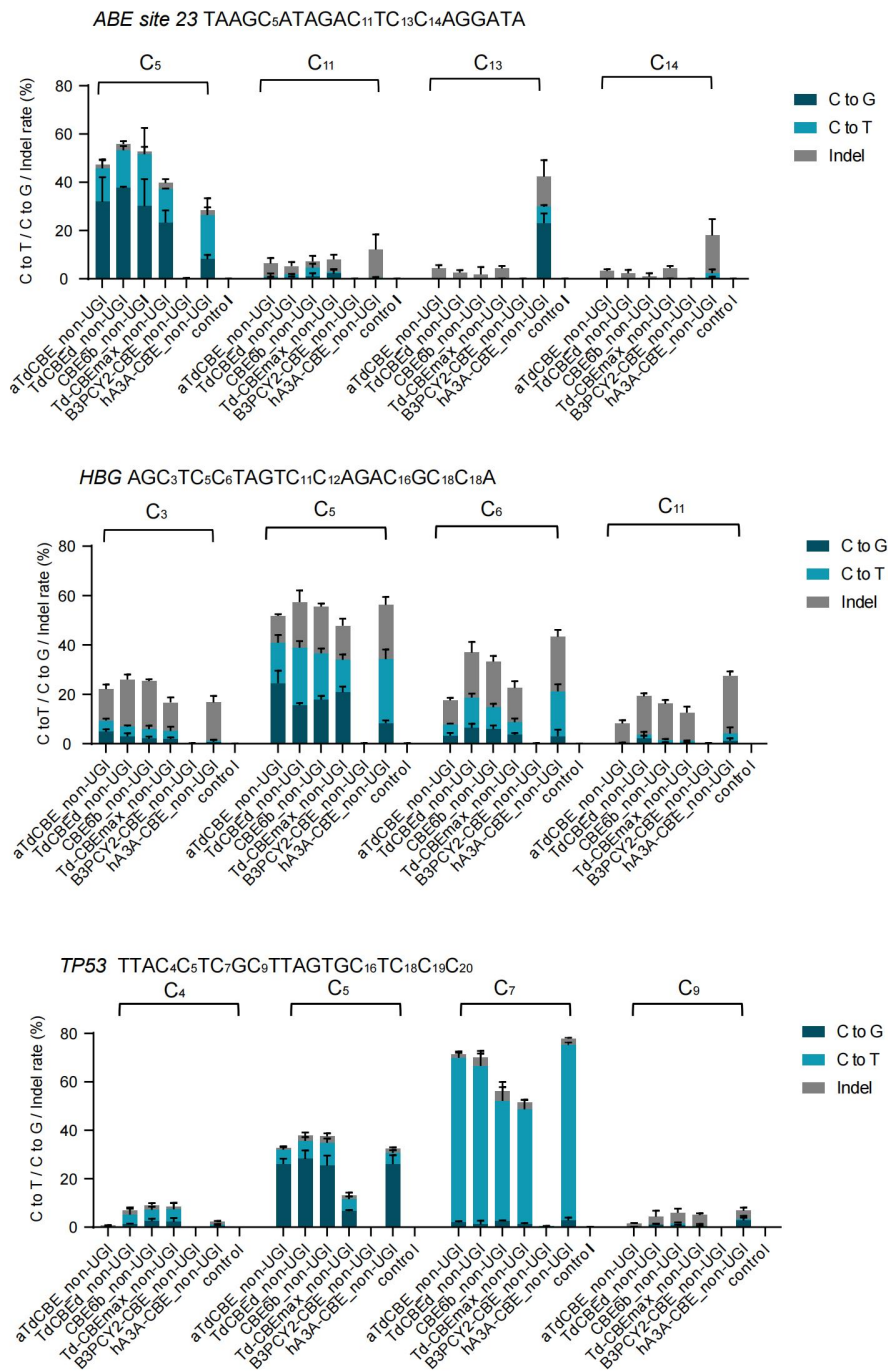


83

84 **Supplementary Fig.5 AjTadA-derived base editors with high specificity**
 85 **in mammalian cells.**

86 **a.** The gRNA-dependent off-target levels at the potential off-target sites. **b.** The
 87 gRNA-independent off-target activity at five R-loops formed by dSaCas9. **c.**
 88 Transcriptome-wide off-target analysis of aTdCBE and TadCBEed. Data are
 89 presented as means \pm S.D. Values represent $n = 3$ independent
 90 biological replicates. All of the above base editors contain UGI.
 91 Source data are provided as a Source Data file.

92

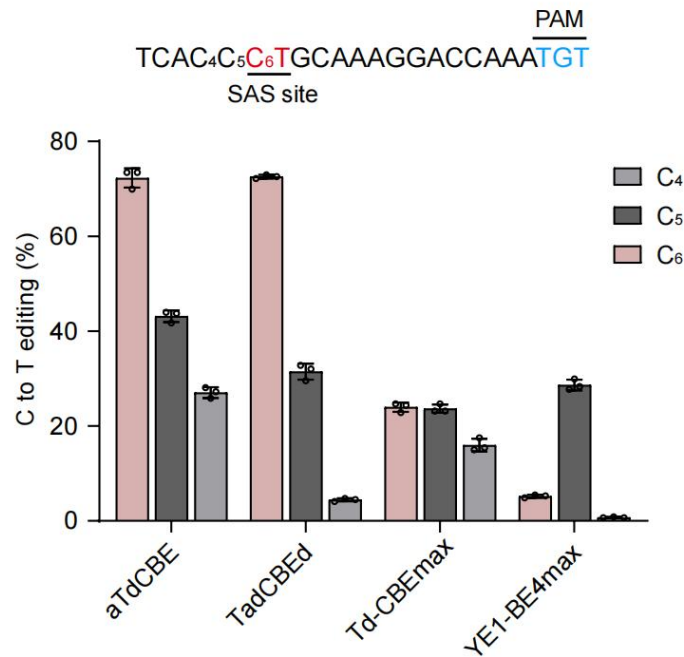


93

94 **Supplementary Fig.6 Compare the editing products of the base**
 95 **editors without UGI at three endogenous loci.**

96 Data are presented as means \pm S.D. Values represent n = 3 independent
 97 biological replicates. All of the above base editors do not contain UGI.

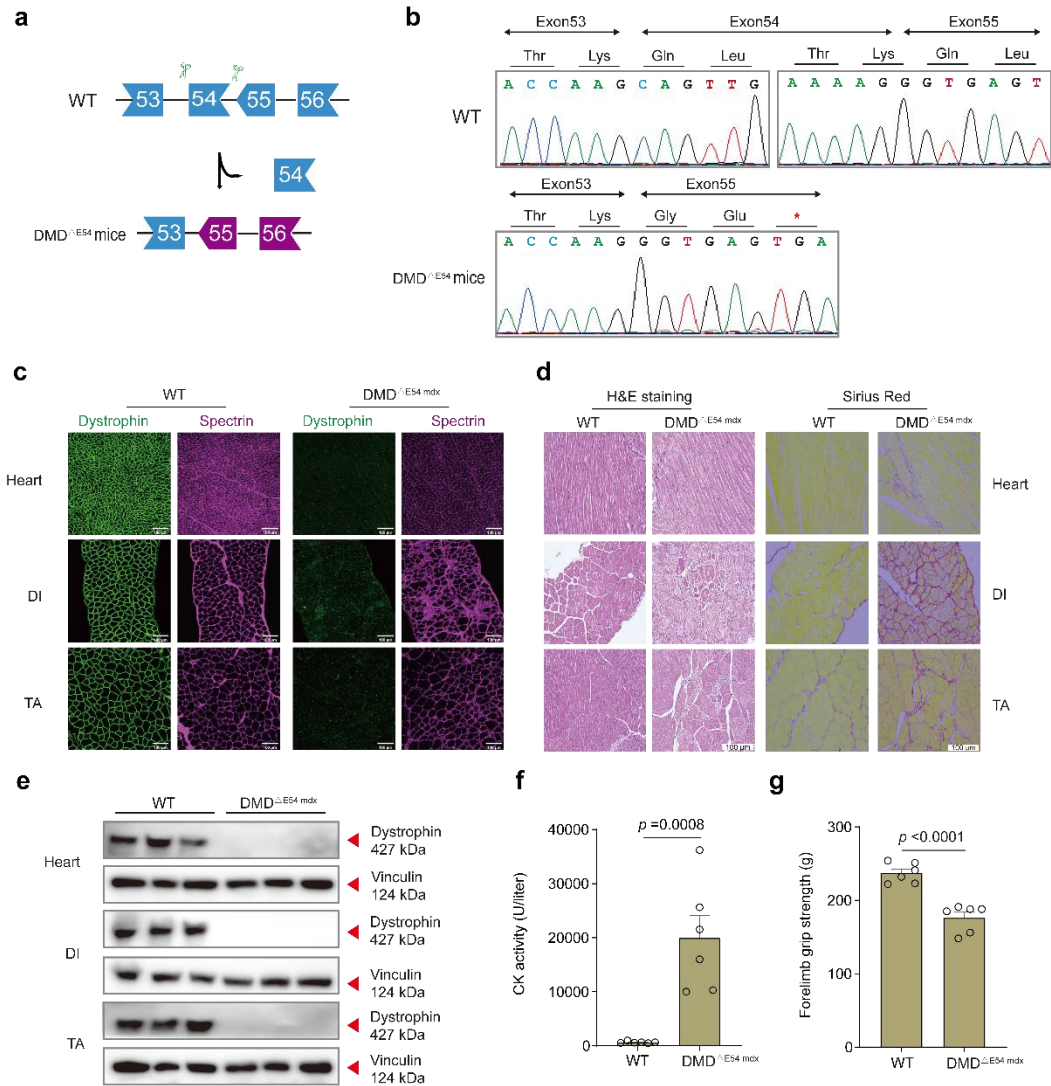
98 Source data are provided as a Source Data file.



99

100 **Supplementary Fig.7 Comparing the editing efficiency of CBEs at the**
 101 **exon 55 SAS of *DMD* gene in HEK293T cells.**

102 SpG Cas9 were used to targeting the SAS-containing sequence with
 103 3'-TGT PAM. Data are presented as means \pm S.D. Values represent n = 3
 104 independent biological replicates. All of the above base editors
 105 contain UGI. Source data are provided as a Source Data file.



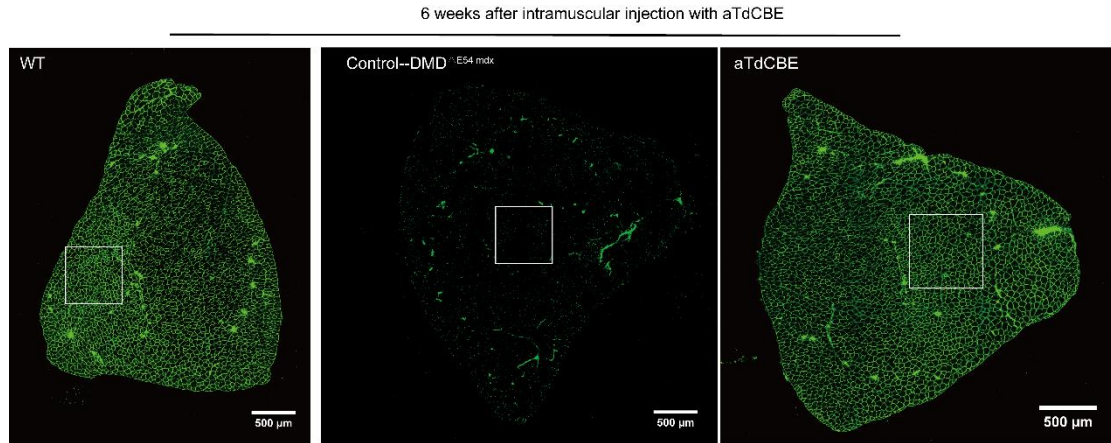
106

107 **Supplementary Fig.8 Establishment and characterization of a**
 108 **humanized DMD mouse model.**

109 **a.** Strategy for generating a humanized DMD mouse model. CRISPR-Cas9
 110 editing was employed to delete human *DMD* exon54. **b.** RT-PCR analysis of
 111 TA muscles to validate deletion of human exon 54. **c.** Dystrophin
 112 immunohistochemistry from indicated muscles of WT and DMD^{ΔE54} mdx mice.
 113 WT mice were derived from crosses between STOCK Tg (DMD) 72Thoen/J
 114 mice (#018900) and mdx mice, which carry a c.2977C>T, p.Gln993* mutation
 115 in exon 23 on Chr.X. Dystrophin (Abcam, ab15277) and spectrin (Millipore,
 116 MAB1622) are shown in green and mangenta, respectively. **d.** Western blot
 117 confirming the absence of dystrophin (Sigma, D8168) in indicated muscle
 118 tissues. **f.** Serum CK, a marker of muscle damage and membrane leakage,
 119 was measured in WT and DMD^{ΔE54} mdx mice. **e.** Sirius red staining and HE
 120 staining of TA, DI, and heart muscle of WT and DMD^{ΔE54} mdx mice. **g.** WT and
 121 DMD^{ΔE54} mdx mice were subjected to forelimb grip strength testing to measure
 122 muscle performance. All mice were 4 weeks old at the time of the experiment.
 123 Data are represented as mean ± s.e.m (n=6 independent biological replicates).

124 Each dot represents an individual mouse. *P*-value was calculated using an
125 unpaired two-tailed Student's *t*-test. Scale bar, 100 μ m. Source data are
126 provided as a Source Data file.

127
128

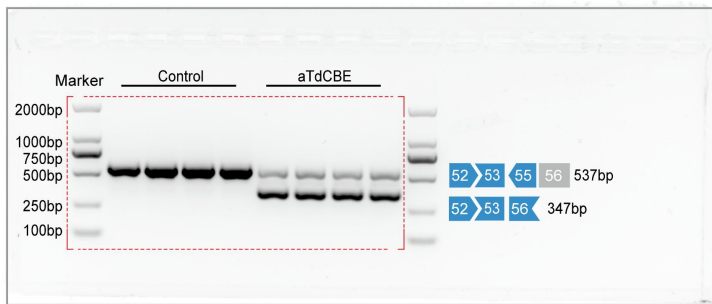


129

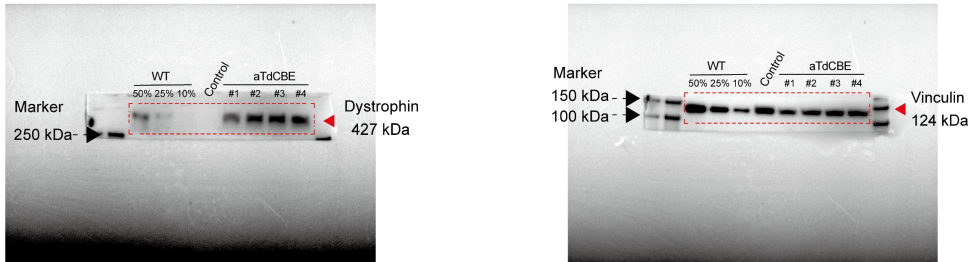
130 **Supplementary Fig.9 Rescue of dystrophin expression following**
131 **intramuscular injection of aTdCBE after 6 weeks.**

132 Dystrophin immunohistochemistry of TA muscle. Control mice were injected
133 with saline. Images shown in both Fig. 4e and Supplementary Fig.8 were
134 obtained from the same tissue at 20x magnification. Fig. 4e showed the local
135 region staining image rather than the reconstituted whole-tissue scanning
136 image in Supplementary Fig.8, and highlighted with white boxes. Dystrophin is
137 shown in green. Scale bar, 500 μ m.

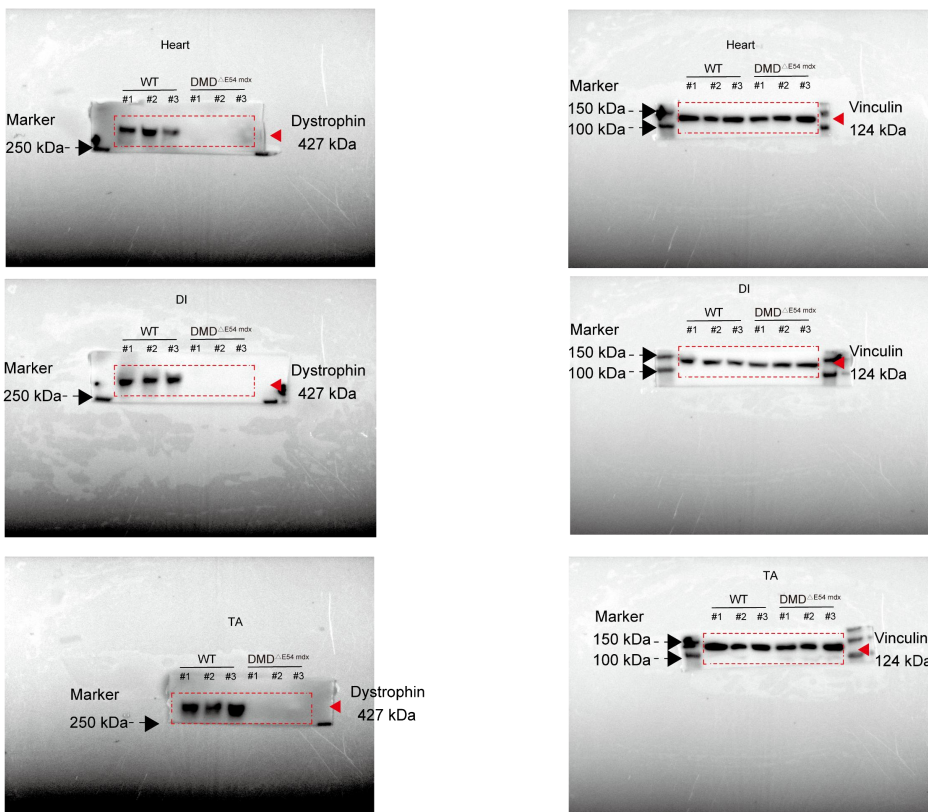
Related to Figure 4d



Related to Figure 4g



Related to Supplementary Figure 8e



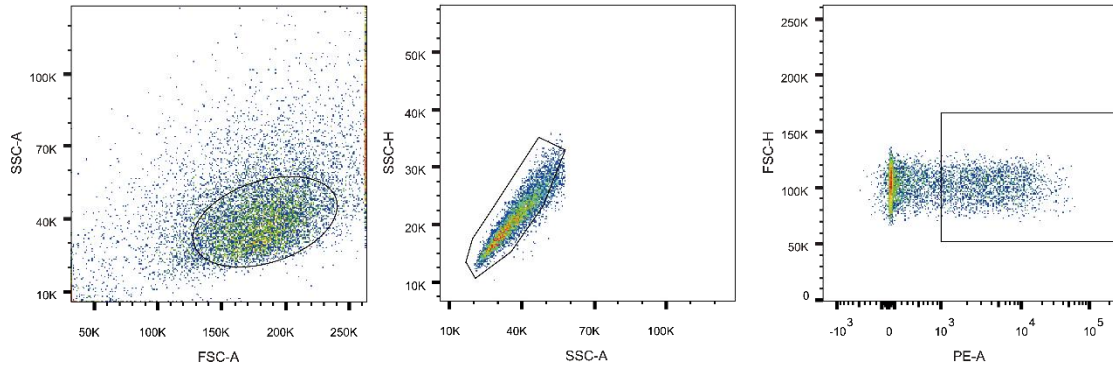
138

139

140

Supplementary Fig.10 Uncropped images.

The red rectangles indicate the cropping location.



141

142

Supplementary Fig.11 Flow cytometry gating strategy.

143

Cell singletons were first gated out via forward scatter (FSC) and side scatter (SSC) parameters. Fluorescent cells were then gated for gene editing

144

analysis.

145